Supporting information for

Transition Metal Dichalcogenide/Multi-walled Carbon Nanotube-based Fibers as Flexible Electrodes for Electrocatalytic Hydrogen Evolution

Bo Chen,‡[b] Gengzhi Sun,‡[c] Jie Wang,‡[b] Guigao Liu,[b] Chaoliang Tan,[b] Ye Chen,[b] Hongfei Cheng,[b] Junze Chen,[b] Qinglang Ma,[b] Ling Huang,[c] Peng Chen,[d] and Hua Zhang*[a,e]

[a]Department of Chemistry, City University of Hong Kong, Hong Kong, China. E-mail: hua.zhang@cityu.edu.hk.

[b]Center for Programmable Materials, School of Materials Science and Engineering, Nanyang Technological University, 50 Nanyang Avenue, Singapore 639798, Singapore.

[c]Key Laboratory of Flexible Electronics (KLOFE) & Institute of Advanced Materials (IAM), National Jiangsu Synergistic Innovation Center for Advanced Materials (SICAM), Nanjing Tech University (NanjingTech), 30 South Puzhu Road, Nanjing 211816, P. R. China.

[d]School of Chemical and Biomedical Engineering, Nanyang Technological University, 70 Nanyang Drive, Singapore 637457, Singapore.

[e]Hong Kong Branch of National Precious Metals Material Engineering Research Center (NPMM), City University of Hong Kong, Hong Kong, China.

‡ These authors contributed equally to this work.

Experimental Section

Chemicals

Potassium tetrachloroplatinate(II) (99.99% trace metals basis), sodium citrate tribasic dehydrate (99.0%), dimethylformamide (DMF, 99.8%, anhydrous), and 20% Pt on charcoal were purchased from Sigma-Aldrich (Steinheim, Germany). Ethanol (99.9%) was purchased from Merck (Darmstadt, Germany). Bulk MoS_2 (10–30 μm) was purchase from Rose Mill (West Hartford, USA). Lithium ion battery electrolyte was purchased from Charslton Technologies Pte Ltd. (International Business Park, Singapore). Lithium foil and copper foil were purchased from ACME Research Support Pte Ltd. (Bukit Batok Street, Singapore. All chemicals were used as received without further purification unless otherwise noted. Milli-Q water (18.2 MΩ·cm) produced by Milli-Q System (Millipore, Billerica, MA) was used in all experiments.

Exfoliation of Transition-Metal Dichalcogenides (TMDs)

The single- or few-layered TMD (*i.e.* MoS_2, $MoSe_2$, TiS_2, and MoS_xSe_{2-x}) nanosheets were prepared using the lithium intercalation method developed by our group.[1] Briefly, lithium intercalation process was performed in an electrochemical test cell with Li foil as anode. The electrolyte was prepared by dissolving 1 M $LiPF_6$ in a mixture of ethyl carbonate and dimethyl carbonate (v:v=1:1). A mixed slurry of MoS_2 powder, acetylene black, and PVDF binder (mass ratio= 8:1:1) was dispersed in N-methylpyrrolidone and used as cathode material, where the resultant mixture was uniformly pasted on a copper foil and dried in vacuum oven at room temperature for 12 h. The lithium intercalation process was carried out in a Neware battery test system, in which the intercalation was then carried out at a discharge current density of 0.05 mA. The resultant Li-intercalated MoS_2) was washed with acetone to eliminate any residual $LiPF_6$ and then ultra-sonicated to exfoliate MoS_2.

Growth of Pt nanoparticles on TMD nanosheets

The growth of Pt nanoparticles on TMD nanosheets was carried out by a photochemical reduction method.[2] Typically, 4 mL of TMD nanosheets solution (0.8 mg) were added into 16 mL aqueous solution in a 20 ml glass vial, which contains pre-dissolved 0.3 mM trisodium citrate and 0.2 mM potassium tetrachloroplatinate. After that, the mixed solution was irradiated under a 150 W

halogen lamp (Fiber-Lite MI-150) with 80% of its maximum intensity for 2 h. The ice bath was used to cool the glass vial and prevent the light-induced overheating. After the photochemical reduction reaction was complete, the solution was centrifuged at 6,500 rpm for 15 min and washed with Milli-Q water for 3 times. Finally, the hybrid nanomaterial was re-dispersed in DMF at a concentration of 2 mg mL^{-1} and then thoroughly ultra-sonicated before use.

Fabrication of fibers and fiber-based electrodes

The multi-walled carbon nanotube (MWCNT) array was grown by vertically aligning them via chemical vapor deposition (CVD) in a quartz tube furnace following our previous work.[3,4] The MWCNT sheet with an areal density of around 2.12 μg cm^{-2} (single layer) was pulled out from the array.[5] Four layers of the sheets with length of ~8.5 cm and width of ~1.5 mm were then stacked on each other and laid on a polytetrafluoroethylene (PTFE) substrate. TMD-based active materials, e.g., Pt-MoS_2 nanosheets, dispersed in DMF (2 mg mL^{-1}) were then added onto the stacked MWCNT sheet by drop casting. The loading amount (weight percentage) of active material in each fiber was calculated as follows, i.e. loading amount = $W_g/(W_g+W_h)$, where W_g and W_h represent weight of guest material (TMD-based materials) and weight of host material (MWCNTs), respectively. The loading amount of TMD-based materials was fixed at 90 wt% unless otherwise noted. The resultant hybrid sheet was then dried in a fume hood, and then carefully peeled off from the PTFE substrate. To obtain the hybrid fiber, one end of the hybrid sheet was pasted on the scotch tape, while the other end was twisted by an electric motor, which rotated at 200 rpm for 2 min. The fiber electrode was fabricated by mounting the as-prepared hybrid fiber (~0.5 cm) onto a glass substrate.[6] A Cu wire was connected to one end of the fiber using Ag paste which was subsequently insulated by the silicon rubber. In order to demonstrate the good flexibility and weavability of hybrid fibers, 10 TMD fibers were woven into a white textile. Before being used for the electrocatalytic water splitting, one end of the hybrid fiber/textile sheet was painted with silver paste.

Electrocatalytic measurements for HER

The electrochemical measurements were obtained by an Autolab electrochemical workstation (PGSTAT302N, Metrohm Autolab, Switzerland). Linear sweep voltammetry (LSV) was carried out in 0.5 M H_2SO_4 or 1 M KOH (deaerated by N_2) at a scan rate of 2 mVs^{-1} from -0.45 to 0.20 V (vs reversible hydrogen electrode (RHE)). The linear regions of the Tafel curves were fitted to the

typical Tafel equation, $\eta = b \log j + a$, where η, b, and j are the overpotential, Tafel slope, and the current density, respectively.[7,8] Pt wire was used as the counter electrode (CE), Ag/AgCl electrode (3 M KCl) was used as the reference electrode (RE), and the as-obtained fiber electrode was used as the working electrode (WE). Proton exchange membrane was used to separate CE from WE and RE. All the measured potentials were referenced to the RHE. Cyclic voltammetry (CV) was conducted by using the same three-electrode setup with a scan rate of 100 mVs^{-1} at room temperature.

Structural characterizations

Scanning electron microscopy (SEM) was performed using a JSM-7600F field-emission scanning electron microscope operated at an accelerating voltage of 5 kV, and the corresponding energy dispersive X-ray spectroscopy (EDS) was recorded at an accelerating voltage of 20 kV. High-resolution transmission electron microscopy (HRTEM) images, dark-field scanning TEM (DF–STEM) images, and selected area electron diffraction (SAED) patterns were collected using a JEM 2100F transmission electron microscope operated under an accelerating voltage of 200 kV. Raman spectra were taken using a WITec CRM200 confocal Raman microscopy system (WITec Instruments Corp, Germany) with the excitation line of 488 nm at room temperature. The spectrometer was pre-calibrated using Raman band of Si at 520 cm^{-1} as the reference.

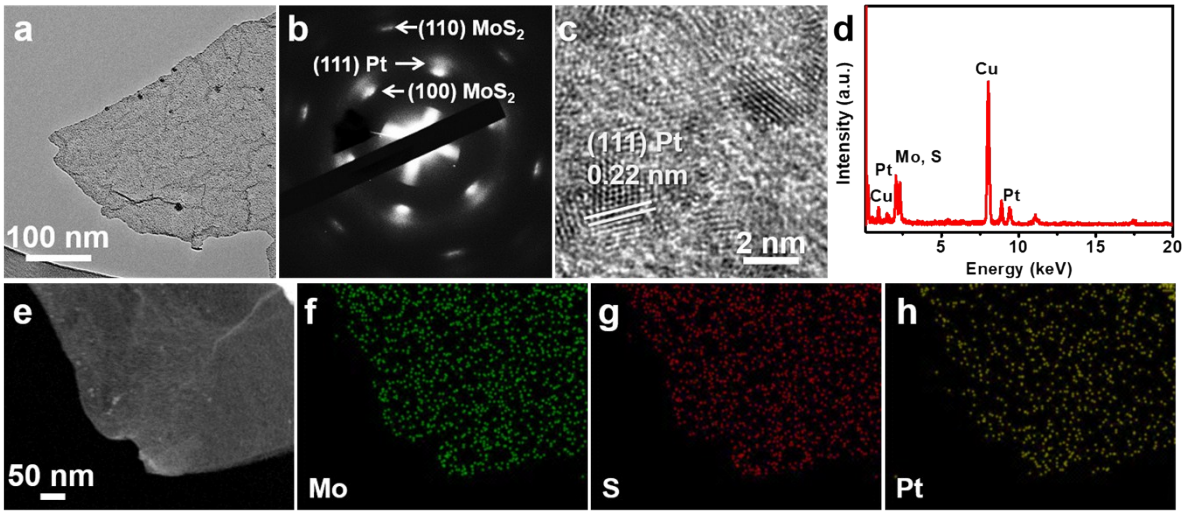

Fig. S1 (a) TEM image, (b) SAED pattern, (c) HRTEM image, (d) EDS spectrum, (e) DF-STEM image, and (f-h) the corresponding EDS elemental mappings of the obtained Pt-MoS_2 nanosheet.

Fig. S1a and b are the TEM image and SAED pattern of a Pt-MoS_2 nanosheet, respectively. As shown in the HRTEM image (Fig. S1c), the lattice spacing of 0.22 nm corresponds to the (111) planes of Pt. The decoration of Pt in Pt-MoS_2 is further confirmed by the EDS spectrum (Fig. S1d), in which the signals of Pt and Mo (S) peaks are located at 2.06 and 2.30 keV, respectively. The DF-STEM image (Fig. S1e) and EDS elemental mappings (Fig. S1f-h) of the Pt-MoS_2 nanosheet reveal the uniform decoration of Pt nanoparticles on the MoS_2 nanosheet.

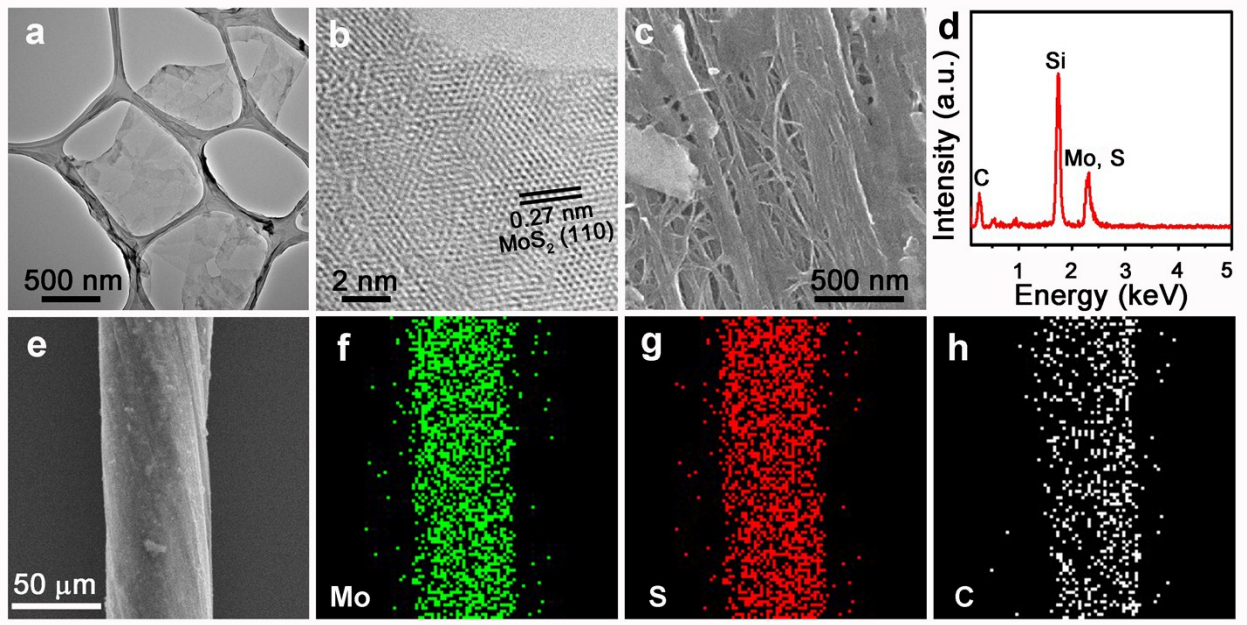

Fig. S2 (a) TEM and (b) HRTEM images of the obtained MoS_2 nanosheets. (c) High-magnification SEM image, (d) EDS spectrum, (e) low-magnification SEM image, and (f-h) the corresponding EDS elemental mappings of a MoS_2/MWCNT fiber.

Fig. S2a and b are TEM and HRTEM images of the obtained MoS_2 nanosheets, respectively. As shown in the HRTEM image (Fig. S2b), the lattice spacing of 0.27 nm corresponds to the (110) planes of MoS_2. Fig. S2c shows a typical high-magnification SEM image of a MoS_2/MWCNT hybrid fiber. The incorporation of MoS_2 nanosheets in the resultant MoS_2/MWCNT hybrid fiber is further confirmed by the signal of Mo (S) peak at 2.30 keV in the EDS spectrum (Fig. S2d). The low-magnification SEM image (Fig. S2e) and EDS elemental mappings (Fig. S2f-h) of the MoS_2/MWCNT hybrid fiber prove the successful incorporation and well distribution of MoS_2 in the hybrid fiber.

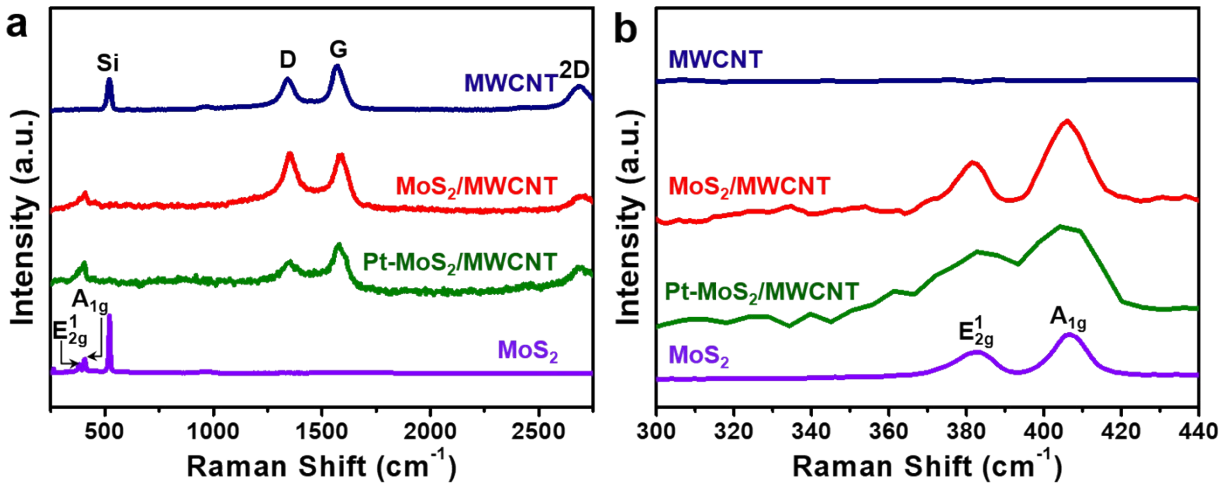

Fig. S3 Raman spectra of the pure MWCNT fiber, MoS_2/MWCNT fiber, Pt-MoS_2/MWCNT fiber, and MoS_2 nanosheets under different grating: (a) 1800 grooves/mm and (b) 600 grooves/mm. The peak at 520 cm^{-1} is associated with crystalline Si substrate.

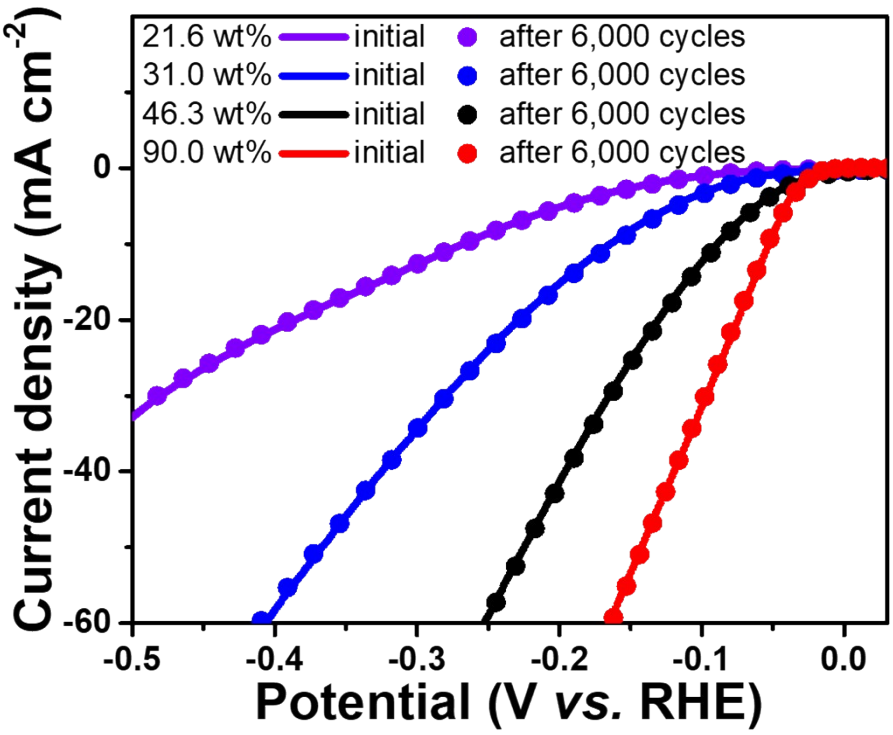

Fig. S4 Polarization curves of Pt-MoS_2/MWCNT fibers with different loading amount (wt%) of Pt-MoS_2 before and after continuous potential sweeps at a scan rate of 100 mVs^{-1} in 0.5 M H_2SO_4.

Polarization curves of Pt-MoS_2/MWCNT fibers with different loading amount (wt%) of Pt-MoS_2 before and after continuous potential sweeps in 0.5 M H_2SO_4 are provided in Fig. S4. Negligible HER current loss is observed for all electrodes with different loading amount (wt%) after 6,000 cycles of cyclic voltammetry from -0.45 to 0.20 V vs. RHE, indicating the excellent durability of Pt-MoS_2/MWCNT fibers with different loading amount (wt%) in acidic environment.

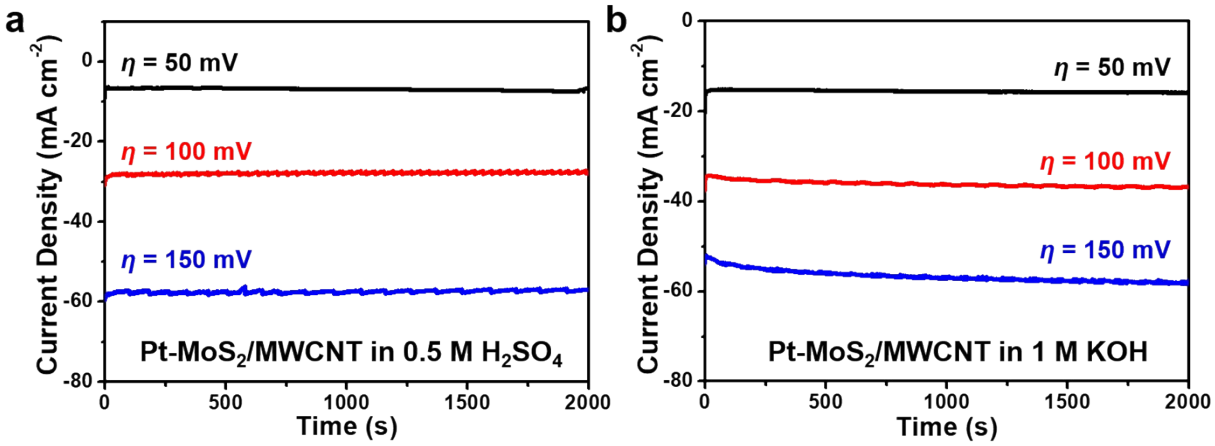

Fig. S5 Time-dependent current density curves of a Pt-MoS_2/MWCNT fiber electrode under different static overpotentials (50, 100, and 150 mV) in (a) 0.5 M H_2SO_4 and (b) 1 M KOH.

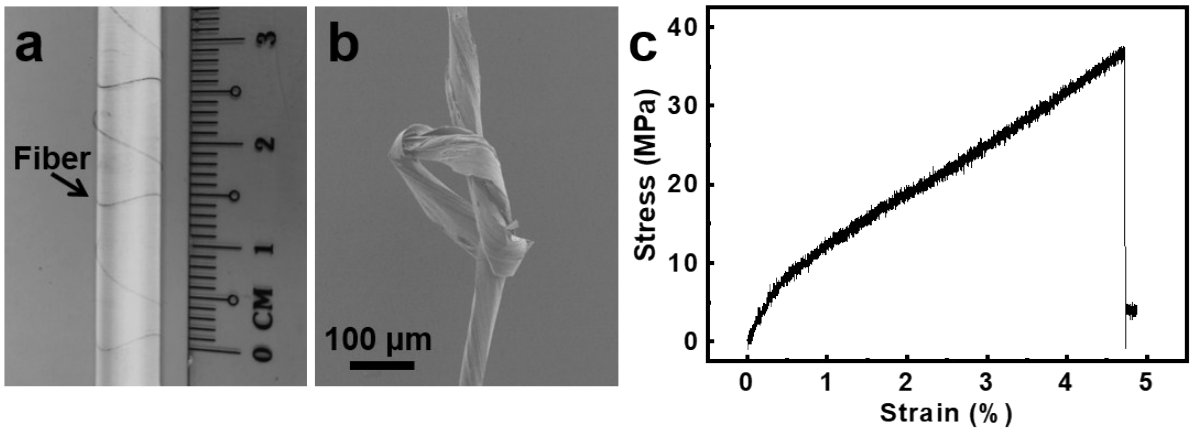

Fig. S6 (a) Photograph of a Pt-MoS_2/MWCNT fiber being wound around a glass rod. (b) SEM image of a Pt-MoS_2/MWCNT fiber being knotted. (c) Stress-strain curve of a Pt-MoS_2/MWCNT fiber.

As shown in Fig. S6, the as-prepared hybrid fibers are highly flexible and can be wound around a glass rod (Fig. S6a) and knotted (Fig. S6b). Stress-strain test (Fig. S6c) shows the obtained fibers possess a tensile strength of over 35 MPa.

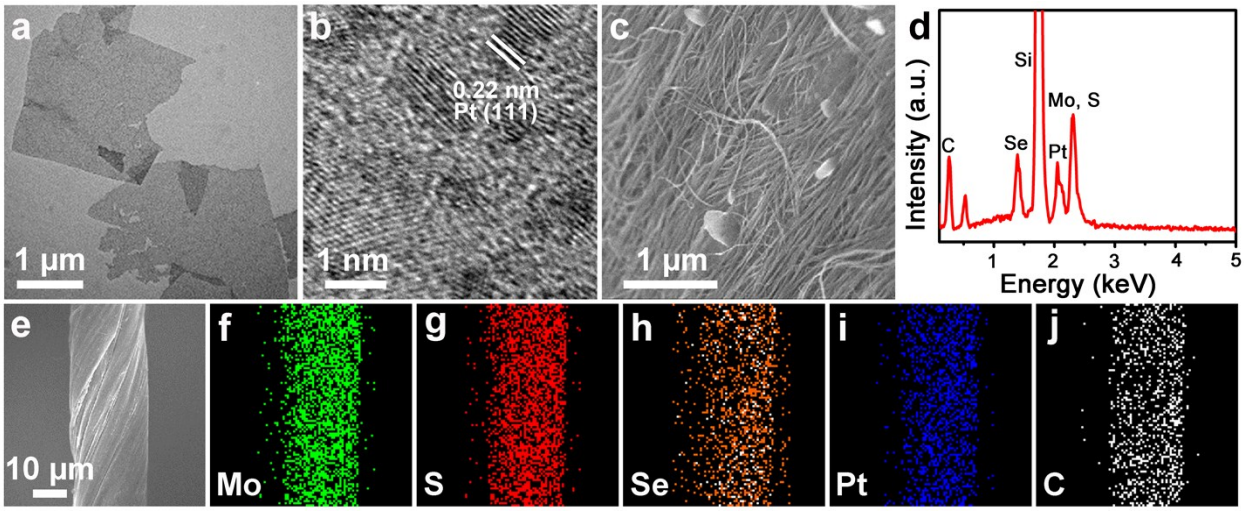

Fig. S7 (a) TEM and (b) HRTEM images of the obtained Pt-MoS_xSe_{2-x} nanosheets. (c) High-magnification SEM image, (d) EDS spectrum, (e) low-magnification SEM image, and (f-j) the corresponding EDS elemental mappings of a Pt-MoS_xSe_{2-x}/MWCNT fiber.

Fig. S7a and b are TEM and HRTEM images of the obtained Pt-MoS_xSe_{2-x} nanosheets, respectively. As shown in the HRTEM image (Fig. S7b), the lattice spacing of 0.22 nm corresponds to the (111) planes of Pt. Fig. S7c shows a typical high-magnification SEM image of a Pt-MoS_xSe_{2-x}/MWCNT hybrid fiber. The incorporation of Pt-MoS_xSe_{2-x} nanosheets in the resultant Pt-MoS_xSe_{2-x}/MWCNT hybrid fiber is further confirmed by the signals of Se, Pt and Mo (S) peaks located at 1.38, 2.06 and 2.30 keV in the EDS spectrum, respectively (Fig. S7d). The low-magnification SEM image (Fig. S7e) and EDS elemental mappings (Fig. S7f-j) of the Pt-MoS_xSe_{2-x}/MWCNT hybrid fiber prove the successful incorporation and well distribution of Pt-MoS_xSe_{2-x} in the hybrid fiber.

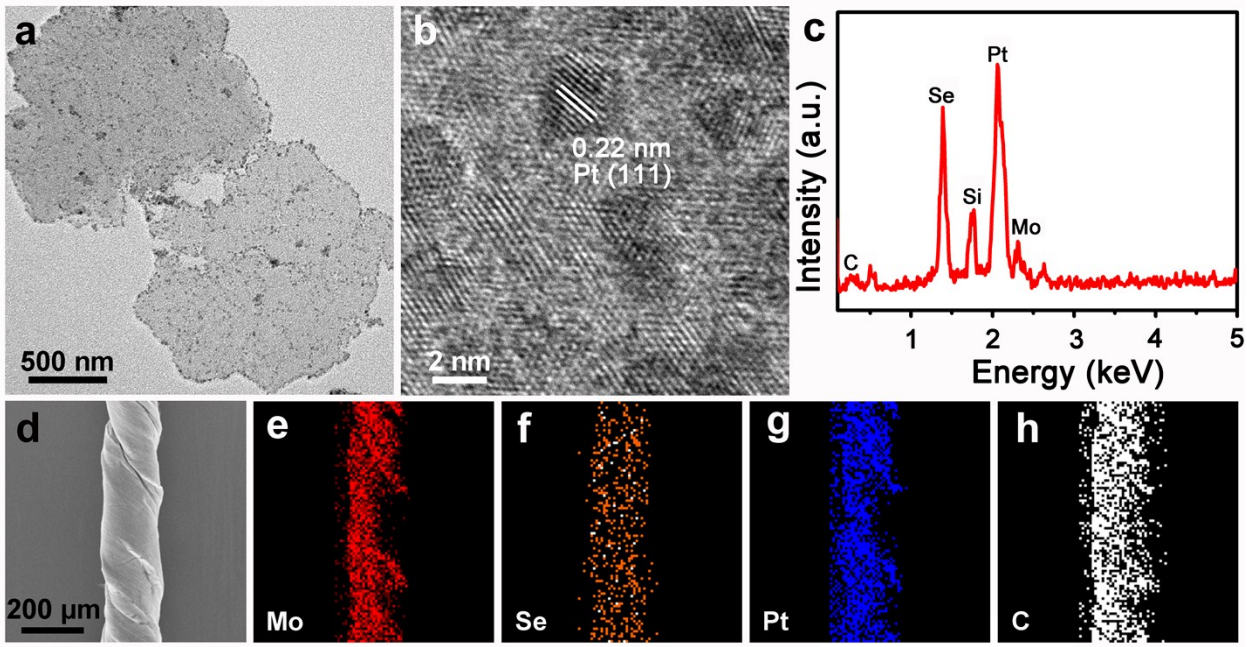

Fig. S8 (a) TEM and (b) HRTEM images of the obtained Pt-$MoSe_2$ nanosheets. (c) EDS spectrum, (d) SEM image, and (e-h) the corresponding EDS elemental mappings of a Pt-$MoSe_2$/MWCNT fiber.

Fig. S8a and b are TEM and HRTEM images of the obtained Pt-$MoSe_2$ nanosheets, respectively. As shown in the HRTEM image (Fig. S8b), the lattice spacing of 0.22 nm corresponds to the (111) planes of Pt. The incorporation of Pt-$MoSe_2$ nanosheets in the resultant Pt-$MoSe_2$/MWCNT hybrid fiber is further confirmed by the signals of Se, Pt and Mo peaks located at 1.38, 2.06 and 2.30 keV in the EDS spectrum, respectively (Fig. S8c). The typical SEM image (Fig. S8d) and EDS elemental mappings (Fig. S8e-h) of the Pt-$MoSe_2$/MWCNT hybrid fiber prove the successful incorporation and well distribution of Pt-$MoSe_2$ in the hybrid fiber.

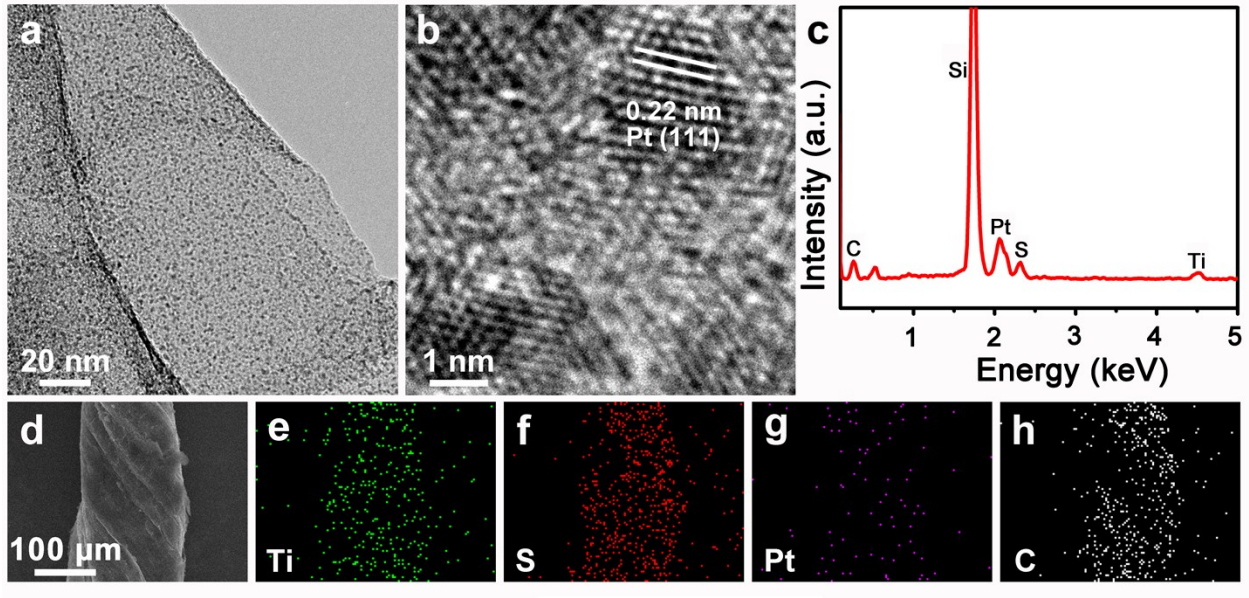

Fig. S9 (a) TEM and (b) HRTEM images of the obtained Pt-TiS_2 nanosheets. (c) EDS spectrum, (d) SEM image, and (e-h) the corresponding EDS elemental mappings of a Pt-TiS_2/MWCNT fiber.

Fig. S9a and b are TEM and HRTEM images of the obtained Pt-TiS_2 nanosheets, respectively. As shown in the HRTEM image (Fig. S9b), the lattice spacing of 0.22 nm corresponds to the (111) planes of Pt. The incorporation of Pt-TiS_2 nanosheets in the resultant Pt-TiS_2/MWCNT hybrid fiber is further confirmed by the signals of Pt, S and Ti peaks located at 2.06, 2.30 and 4.51 keV in the EDS spectrum, , respectively (Fig. S9c). The typical SEM image (Fig. S9d) and EDS elemental mappings (Fig. S9e-h) of the Pt-TiS_2/MWCNT hybrid fiber prove the successful incorporation and well distribution of Pt-TiS_2 in the hybrid fiber.

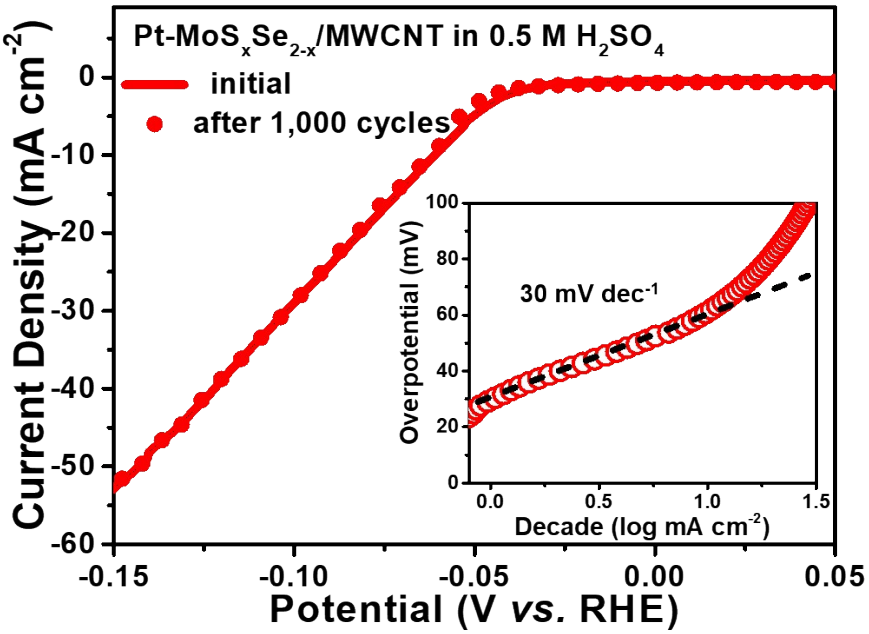

Fig. S10 Polarization curves of a Pt-MoS_xSe_{2-x}/MWCNT fiber before and after continuous potential sweeps at a scan rate of 100 mVs^{-1} in 0.5 M H_2SO_4. Negligible HER current loss was observed after 1,000 cycles of cyclic voltammetry from -0.45 to 0.20 V *vs.* RHE. Inset: the corresponding Tafel plot of the Pt-MoS_xSe_{2-x}/MWCNT fiber before continuous potential sweeps. The dashed line shows the linear region used to estimate the Tafel slope (30 mV dec^{-1}).

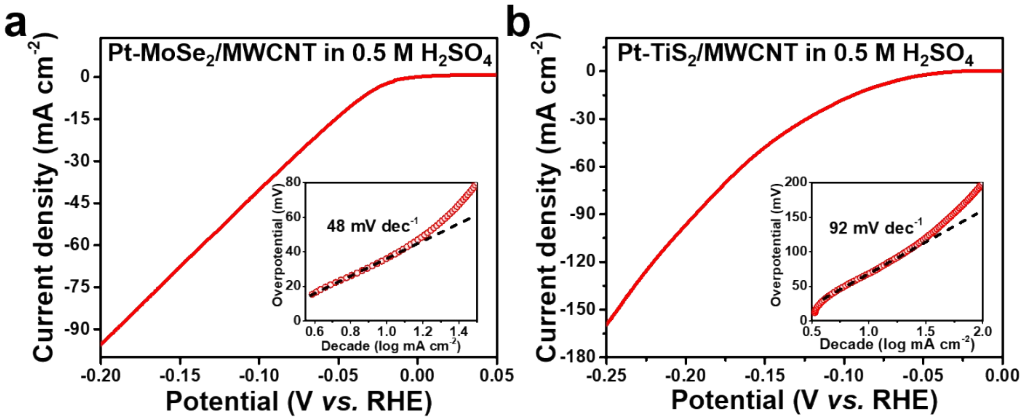

Fig. S11 Polarization curves of the (a) Pt-$MoSe_2$/MWCNT fiber and (b) Pt-TiS_2/MWCNT fiber at a scan rate of 2 mV s^{-1} in 0.5 M H_2SO_4. Insets: the corresponding Tafel plots. The dashed lines show the linear regions used to estimate the Tafel slopes.

Pt-$MoSe_2$/MWCNT and Pt-TiS_2/MWCNT fibers were also used as electrodes for HER. As shown in Fig. S11a, the Tafel slope and overpotential at j=10 mA cm^{-2} of the obtained Pt-$MoSe_2$/MWCNT fiber are 48 mV dec^{-1} and 41 mV, respectively. As shown in Fig. S11b, Tafel slope and overpotential at j=10 mA cm^{-2} of the obtained Pt-TiS_2/MWCNT fiber are 92 mV dec^{-1} and 80 mV, respectively. The HER activities of various fiber electrodes are summarized in Table S1.

Table S1. Summary of HER activities of various fiber electrodes.

Catalyst	Electrolyte	Overpotential at j=10 mA cm^{-2} (mV)	Overpotential at j=30 mA cm^{-2} (mV)	Tafel slope (mV dec^{-1})	Tafel region (mV)	Exchange current density (mA cm^{-2})
MWCNT fiber	0.5 M H_2SO_4	—	—	148	250-330	0.0005
MoS_2/MWCNT fiber	0.5 M H_2SO_4	287	374	118	170-280	0.0413
Pt-MoS_2/MWCNT fiber	**0.5 M H_2SO_4**	**40**	**72**	**30**	**20-35**	**0.4554**
Pt-MoS_xSe_{2-x}/MWCNT fiber	0.5 M H_2SO_4	63	101	30	32-53	0.0975
Pt-$MoSe_2$/MWCNT fiber	0.5 M H_2SO_4	41	81	48	19-35	0.5352
Pt-TiS_2/MWCNT fiber	0.5 M H_2SO_4	80	124	92	30-112	1.8571
Pt-MoS_2/MWCNT fiber	1 M KOH	31	74	40	0-15	3.1622

The HER activities of various fiber electrodes are summarized in Table S1. Among all fibers, the Pt-MoS_2/MWCNT fiber exhibits the best HER performance with the lowest values of overpotential at j=10 mA cm^{-2} (40 mV), overpotential at j=30 mA cm^{-2} (72 mV), and Tafel slope (30 mV dec^{-1}) in 0.5 M H_2SO_4. The Pt-MoS_2/MWCNT fiber also possesses excellent catalytic activity in basic electrolyte with an overpotential of 31 mV at current density of 10 mA cm^{-2} and Tafel slope of 40 mV dec^{-1}.

Table S2. Comparison of HER performances of Pt-TMD/MWCNT fibers in this work and other previously reported TMD-based catalysts.

Catalyst	Overpotential (mV) at j=10 mA cm^{-2}	Tafel slope ($mV\ dec^{-1}$)	Ref.
Pt-MoS_2/MWCNT fiber	**40**	**30**	**This work**
Pt-MoS_xSe_{2-x}/MWCNT fiber	63	30	This work
Pt-$MoSe_2$/MWCNT fiber	41	48	This work
Pt-TiS_2/MWCNT fiber	80	92	This work
Au@MoS_2 nanocomposite	178	43	[9]
Pd-MoS_2	89	80	[10]
Ir/MoS_2	44	32	[11]
Pt-MoS_2	~140	96	[12]
Co-doped MoS_2 foam	156	74	[13]
MoS_2 nanodots	173	53	[14]
Vertically aligned ultrasmall monolayer MoS_2	126	67	[15]
P-1T-MoS_2	154	43	[16]
MoS_2 with S-vacancies	320	102	[17]
MoS_2-BP nanosheets	85	68	[18]
MoS_2 with strain and S-vacancies	170	60	[19]
MoS_2 nanoflower-decorated reduced graphene oxide paper	240	95	[20]
MoS_2/MWCNT	185	44.6	[21]
Defect-rich MoS_2 nanosheets	200	50	[22]
Vertically MoS_2 aligned layers	>400	75	[23]
2H MoS_2 nanosheets	300	75-85	[24]

The comparison of HER performances of Pt-TMD/MWCNT fibers in this work and other previously reported TMD-based catalysts is summarized in Table S2. Due to the unique structure and synergetic interaction between MWCNTs and Pt-MoS_2 nanosheets, the HER performances of our Pt-TMD/MWCNT fibers are comparable with or even better than many other representative TMD-based catalysts. In particular, the Pt-MoS_2/MWCNT fiber exhibits best HER performance with an overpotential of 40 mV at current density of 10 mA cm^{-2} and Tafel slope of about 30 mV dec^{-1} among the catalysts listed in Table S2.

Reference

1 Z. Y. Zeng, T. Sun, J. X. Zhu, X. Huang, Z. Y. Yin, G. Lu, Z. X. Fan, Q. Y. Yan, H. H. Hng and H. Zhang, *Angew. Chem. Int. Ed.*, 2012, **51**, 9052-9056.

2 X. Huang, Z. Zeng, S. Bao, M. Wang, X. Qi, Z. Fan and H. Zhang, *Nat. Commun.*, 2013, **4**, 1444.

3 G. Z. Sun, Y. X. Huang, L. X. Zheng, Z. Y. Zhan, Y. N. Zhang, J. H. L. Pang, T. Wu and P. Chen, *Nanoscale*, 2011, **3**, 4854-4858.

4 G. Z. Sun, L. X. Zheng, J. An, Y. Z. Pan, J. Y. Zhou, Z. Y. Zhan, J. H. L. Pang, C. K. Chua, K. F. Leong and L. Li, *Nanoscale*, 2013, **5**, 2870-2874.

5 G. Z. Sun, X. Zhang, R. Z. Lin, J. Yang, H. Zhang and P. Chen, *Angew. Chem. Int. Ed.*, 2015, **54**, 4651-4656.

6 G. Z. Sun, J. Y. Zhou, F. Yu, Y. N. Zhang, J. H. L. Pang and L. X. Zheng, *J. Solid State Electrochem.*, 2012, **16**, 1775-1780.

7 J. Xie, H. Zhang, S. Li, R. Wang, X. Sun, M. Zhou, J. Zhou, X. W. D. Lou and Y. Xie, *Adv. Mater.*, 2013, **25**, 5807-5813.

8 M. Kim, M. A. R. Anjum, M. Lee, B. J. Lee and J. S. Lee, *Adv. Funct. Mater.*, 2019, **29**, 1809151.

9 Z. Liu, X. Zhang, Y. Gong, Q. Lu, Z. Zhang, H. Cheng, Q. Ma, J. Chen, M. Zhao, B. Chen, Y. Chen, X.-J. Wu, P. Yin, L. Gu, Y. Du and H. Zhang, *Nano Res.*, 2019, **12**, 1301-1305.

10 Z. Luo, Y. Ouyang, H. Zhang, M. Xiao, J. Ge, Z. Jiang, J. Wang, D. Tang, X. Cao, C. Liu and W. Xing, *Nat. Commun.*, 2018, **9**, 2120.

11 S. Wei, X. Cui, Y. Xu, B. Shang, Q. Zhang, L. Gu, X. Fan, L. Zheng, C. Hou, H. Huang, S. Wen and W. Zheng, *ACS Energy Lett.*, 2019, **4**, 368-374.

12 J. Deng, H. Li, J. Xiao, Y. Tu, D. Deng, H. Yang, H. Tian, J. Li, P. Ren and X. Bao, *Energy Environ. Sci.*, 2015, **8**, 1594-1601.

13 J. Deng, H. Li, S. Wang, D. Ding, M. Chen, C. Liu, Z. Tian, K. S. Novoselov, C. Ma, D. Deng and X. Bao, *Nat. Commun.*, 2017, **8**, 14430.

14 C. L. Tan, Z. M. Luo, A. Chaturvedi, Y. Q. Cai, Y. H. Du, Y. Gong, Y. Huang, Z. C. Lai, X. Zhang, L. R. Zheng, X. Y. Qi, M. H. Goh, J. Wang, S. K. Han, X. J. Wu, L. Gu, C. Kloc and H. Zhang, *Adv. Mater.*, 2018, **30**, 1705509.

15 L.-B. Huang, L. Zhao, Y. Zhang, Y.-Y. Chen, Q.-H. Zhang, H. Luo, X. Zhang, T. Tang, L. Gu and J.-S. Hu, *Adv. Energy Mater.*, 2018, **8**, 1800734.

16 Y. Yin, J. Han, Y. Zhang, X. Zhang, P. Xu, Q. Yuan, L. Samad, X. Wang, Y. Wang, Z. Zhang, P. Zhang, X. Cao, B. Song and S. Jin, *J. Am. Chem. Soc.*, 2016, **138**, 7965-7972.

17 C. Tsai, H. Li, S. Park, J. Park, H. S. Han, J. K. Nørskov, X. Zheng and F. Abild-Pedersen, *Nat. Commun.*, 2017, **8**, 15113.

18 R. He, J. Hua, A. Zhang, C. Wang, J. Peng, W. Chen and J. Zeng, *Nano Lett.*, 2017, **17**, 4311-4316.

19 H. Li, C. Tsai, A. L. Koh, L. Cai, A. W. Contryman, A. H. Fragapane, J. Zhao, H. S. Han, H. C. Manoharan, F. Abild-Pedersen, J. K. Nørskov and X. Zheng, *Nat. Mater.*, 2016, **15**, 48-53.

20 C.-B. Ma, X. Qi, B. Chen, S. Bao, Z. Yin, X.-J. Wu, Z. Luo, J. Wei, H.-L. Zhang and H. Zhang, *Nanoscale*, 2014, **6**, 5624-5629.

21 Y. Yan, X. Ge, Z. Liu, J.-Y. Wang, J.-M. Lee and X. Wang, *Nanoscale*, 2013, **5**, 7768-7771.

22 J. Xie, H. Zhang, S. Li, R. Wang, X. Sun, M. Zhou, J. Zhou, X. W. Lou and Y. Xie, *Adv. Mater.*, 2013, **25**, 5807-5813.

23 D. Kong, H. Wang, J. J. Cha, M. Pasta, K. J. Koski, J. Yao and Y. Cui, *Nano Lett.*, 2013, **13**, 1341-1347.
24 D. Voiry, M. Salehi, R. Silva, T. Fujita, M. Chen, T. Asefa, V. B. Shenoy, G. Eda and M. Chhowalla, *Nano Lett.*, 2013, **13**, 6222-6227.